An electrically conductive silver-polyacrylamide-alginate hydrogel composite for soft electronics

Yunsik Ohm[1,2,5], Chengfeng Pan[1,2,5], Michael J. Ford[1,2], Xiaonan Huang[1,2], Jiahe Liao[1,3], Carmel Majidi[1,2,3,4,*]

[1]Soft Machines Lab, Carnegie Mellon University, Pittsburgh, PA 15213, USA.

[2]Mechanical Engineering, Carnegie Mellon University, Pittsburgh, PA 15213, USA.

[3]Robotics Institute, Carnegie Mellon University, Pittsburgh, PA 15213, USA.

[4]Materials Science & Engineering, Carnegie Mellon University, Pittsburgh, PA 15213, USA.

[5]These authors contributed equally: Yunsik Ohm, Chengfeng Pan.

*To whom correspondence should be addressed; E-mail: cmajidi@andrew.cmu.edu.

Abstract

Hydrogels offer tissue-like compliance, stretchability, fracture toughness, ionic conductivity, and compatibility with biological tissues. However, their electrical conductivity (<100 S cm^{-1}) is inadequate for digital circuits and applications in bioelectronics. Furthermore, efforts to increase conductivity by using hydrogel composites with conductive fillers have led to compromises in compliance and deformability. Here, we report a hydrogel composite that has a high electrical conductivity (>350 S cm^{-1}) and is capable of delivering direct current while maintaining soft compliance (Young's modulus $<$ 10 kPa) and deformability. Micrometre-sized silver flakes are suspended in a polyacrylamide-alginate hydrogel matrix and, after going through a partial dehydration process, the flakes form percolating networks that are electrically conductive and robust to mechanical deformations. To illustrate the capabilities of our silver-hydrogel, we use the material in a stingray-inspired swimmer and a neuromuscular electrical stimulation electrode.

Soft electronics that exhibit high electrical conductivity and match the compliance of biological tissue are important in the development of wearable computing[1,2], soft sensors[3,4]/actuators[5], energy storage/generation devices[6,7], and stretchable displays[8,9]. A variety of material architectures have been used to create soft and stretchable electronics, including deterministic (e.g., wavy, serpentine) structures[10,11], soft microfluidic channels[12,13], and conductive composites or polymers[14–16]. However, these conductive materials have intrinsic limitations, such as relatively high Young's modulus (>>1 MPa in some cases) or limited deformability, and thus are not ideally suited for many emerging applications related to bioelectronic systems (e.g., interfacing with biological tissues). Recently, researchers have demonstrated conductive elastomers with enhanced stretchability and compliance by incorporating microdroplets of liquid metal alloys such as eutectic gallium indium (EGaIn)[17,18]. In particular, a highly stretchable and conductive polymer composite has been developed using silver and EGaIn particles embedded in an ethylene vinyl acetate copolymer[18]. Although EGaIn-based polymer composites exhibit an encouraging combination of high conductivity, stretchability, and compliance, they require a large volume fraction of metallic filler and their Young's modulus (~0.1-1 MPa) is greater than the modulus of soft gels and biological materials (roughly 1-10 kPa), e.g., adipose (body fat) tissue[19]. In this respect, there remains to be a stretchable conductive polymer with enough electrical conductivity to support broad use in electronics combined with a sufficiently low Young's modulus to match the compliance of soft biological tissue.

Hydrogels are a promising candidate for soft electronics since they have similar mechanical properties to a range of biological materials and soft tissues[20,21], including epidermal skin[22], brain[23], spinal cord[24], and cardiac tissue[25]. Recent research has highlighted various aspects of hydrogels, including their high fracture toughness, tissue-like Young's modulus ($<10^2$ kPa), high-water content (>75%), ionic conductivity, bioactivity, and biocompatibility[21,26]. These properties enable unique applications in bioelectronics[27] and soft robotics[28], including soft-matter sensors[9,29] and actuators[30]. However, hydrogels have an intrinsic ionic conductivity (10^{-5} to 10^{-1} S cm^{-1})[31–33] that is 6-9 orders of magnitude lower than the conductivity of metals), and is inadequate for digital and power electronics[34].

To improve their electrical properties, hydrogel matrices have been filled with conductive materials such as metallic fillers (e.g., nanowires or micro/nanoparticles)[35–38], carbon-based conductive materials (e.g., carbon nanotubes or graphene)[39,40], and intrinsically conducting polymers (e.g., PEDOT:PSS or PANI)[3,34,41,42]. These composites demonstrate the potential for engineering hydrogels that are both electrically conductive ($\sim10^{-5}$-10^1 S cm^{-1}) and have tissue-like mechanical compliance. However, there is a trade-off between improved electrical conductivity and lowered compliance and deformability in these conductive hydrogel composites. For instance, a pure PEDOT:PSS hydrogel[34] has been developed with electrical conductivity (~40 S cm^{-1}) but high Young's modulus (~2 MPa) and low maximum strain limit

(<35% strain), while a soft graphene hydrogel[40] has been synthesized with favourable mechanical properties (Young's modulus of 50 kPa) but low electrical conductivity (~10^{-4} S cm^{-1}).

In this Article, we report a method for creating an electrically conductive hydrogel composite that has high electrical conductivity (374 S cm^{-1}), low Young's modulus (<10 kPa) that matches soft biomaterials like adipose tissue[19], and high stretchability (250% strain). We use a polyacrylamide (PAAm)-alginate hydrogel that is embedded with a low concentration of silver (Ag) flakes. Electrical conductivity is created via a partial dehydration process[34] in which a moderate portion of water is removed in order to induce percolation and create electrically conductive pathways (Fig. 1a and 1b). Because the composite has a low concentration of metallic filler, it exhibits only modest hysteresis between loading and unloading cycles. The combination of high conductivity, low Young's modulus, high electrical stability, and high stretchability enables the hydrogel composite to occupy a unique place in the design space of electrically conductive soft materials for applications in soft robotics, bioelectronics, and wearable electronics (Fig. 1c, Supplementary Figure 1, and Supplementary Table 1). To highlight potential applications of this soft conductor, we demonstrated a LED circuitry that shows high mechanical compliance (Fig. 1d and Supplementary Figure 2), a stingray-inspired soft swimmer where the shape-memory alloy (SMA) muscle was actuated with power transmitted through the conductive hydrogel composite, and a neuromuscular electrical stimulation electrode that can successfully deliver high frequency electrical signals generated by a commercial stimulator.
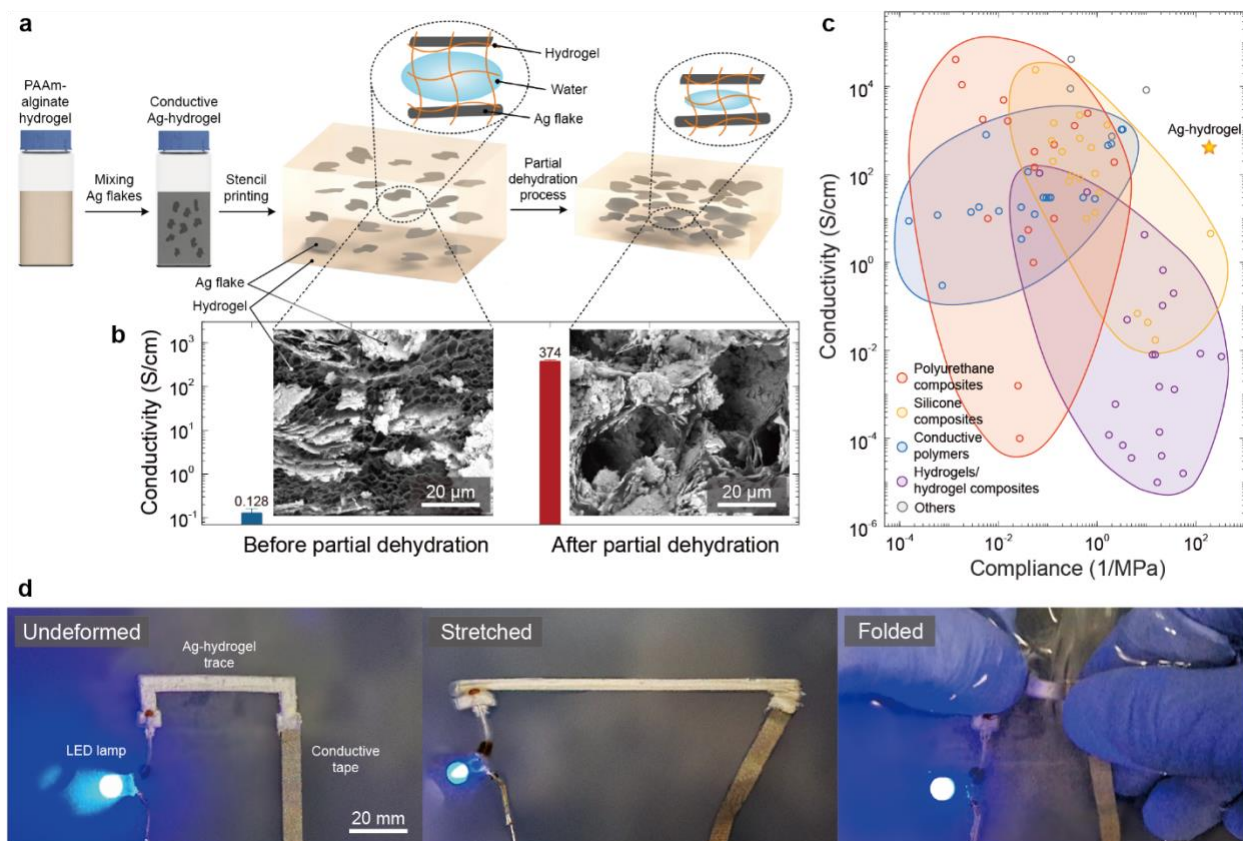
Fig. 1 | Soft, stretchable, and electrically conductive hydrogel composite. a, Composition and synthesis of the conductive hydrogel composite composed of micrometre-sized silver (Ag) flakes and polyacrylamide (PAAm)-alginate hydrogel (Ag-hydrogel). **b**, Conductivity of the Ag-hydrogel composite and micrographs of the composite before and after the controlled partial dehydration process. The error bars are the standard deviation for $N = 3$ samples. **c**, An Ashby-style plot comparing conductivity and compliance of the Ag-hydrogel with other soft conductors (data points are from references mentioned in Supplementary Figure 1 and Supplementary Table 1). **d**, Undeformed (left), stretched (centre), and folded (right) circuitry made of the stencil-printed Ag-hydrogel to power LED lamp (Supplementary Figure 2 and Supplementary Movie 1).

Ag-hydrogel composite

The highly conductive hydrogel composite was fabricated by controlling assembly and percolation of silver (Ag) flakes within a polyacrylamide (PAAm)-alginate hydrogel matrix. Ag flakes were utilized since silver has high electrical conductivity and the high aspect ratio of the flakes permits morphologies that allow for greater electrical conductivity compared to networks of other conductive particles with similar volume concentration. The key step in achieving high electrical conductivity is to perform a partial dehydration of the hydrogel matrix, which enables the Ag flakes to form percolation pathways that remain stable when the composite is stretched or rehydrated (Fig. 1a). The composition and synthesis of the PAAm-alginate gel matrix was adopted from previous work by Sun *et al.*[43]. However, for our system, we did not replace the sodium ion (Na$^+$) of the alginate with other multivalent cations, such as calcium ion (Ca^{2+}) as had been previously done. Although the material isn't ionically crosslinked by multivalent cations, it shows enhanced stretchability and toughness through the formation of a double-network hydrogel matrix enabled by mechanical and chemical interactions between two hydrogel matrices[43,44].

After stencil printing (Supplementary Figure 3) and before performing the partial dehydration, the Ag-hydrogel is ionically conductive with a low conductivity (~0.13 S cm^{-1}). At this stage of the fabrication process, the volume fraction of the Ag filler (5 vol%) is insufficient for percolation. The reason for using such a low volume fraction of Ag flakes instead of adding enough Ag fillers to exceed percolation threshold is that the presence of a large amount of Ag will suppress the double crosslinking process of the hydrogel matrix. As observed in cross-section images taken by scanning electron microscopy (SEM), adjacent Ag flakes are separated by the surrounding hydrogel matrix and don't form a connected network (Fig. 1b left inset). Given that the hydrogel matrix is composed of a hydrophilic polymer network with ~90 vol% of water, partial dehydration reduces the water content and allows for the formation of a percolating network of Ag flakes (Fig. 1b right inset and Supplementary Figure 4). Concomitantly, we observed that the electrical conductivity of the composite increased from 0.128 S cm^{-1} to 374 S cm^{-1} after dehydration (Fig. 1b). The partial dehydration process enables the hydrogel composite to achieve high electrical conductivity, while maintaining tissue-like mechanical properties, i.e., low Young's modulus and high stretchability (Fig. 1c).

We measured electrical resistance changes of the Ag-hydrogel composites with different amounts of Ag content *in-situ* during the partial dehydration to better understand the effect of drying (Fig. 2a and Supplementary Figure 5). The Ag-hydrogel composite specimens (40 mm × 3 mm × 0.7 mm) were stencil-printed on a PAAm-alginate hydrogel substrate using a polydimethylsiloxane (PDMS) mask (Sylgard 184; Dow Corning) (see Methods). Fig. 2a shows the evolution in resistance as a function of partial drying time and the volumetric conductivity of the composites at 0 min and 90 min for the specimen with Ag content

of 5 vol%. Initially, the resistance was on the order of kiloohms, with a corresponding conductivity of 0.128 ± 0.0348 S/cm for $N = 3$ samples, which indicates no electrical conductivity but ionic conductivity as the value of conductivity was more similar to an unfilled hydrogel[45]. The resistance of the Ag-hydrogel decreased exponentially after 10-15 minutes of drying, as electrically conductive paths began to form (Supplementary Figure 4). As we described previously, Ag flakes do not initially form conductive pathways due to the high initial water content. The evaporation of water in the hydrogel matrix may facilitate intimate contact and adhesion between adjacent Ag flakes aggregate, thereby allowing for the formation of electrically conductive pathways. After exceeding the percolation threshold, the electrical conductivity reaches a saturation plateau. At this stage, the resistance is decreased to $1.14 \pm 0.359 \ \Omega$ after 90 minutes, and the corresponding volumetric conductivity reaches 374 ± 30.8 S cm^{-1} for $N = 3$ samples. Higher volumetric Ag content after partial dehydration was observed as the cross-section area of the specimen decreased from 1.76 mm^2 to 1.38 mm^2 after 90 minutes of drying (Supplementary Figure 5b), which corresponds to an increase in the effective Ag content from 5.00 vol% to 6.07 vol% and a decrease in the effective water content from 81.9 vol% to 78.1 vol%. Similar trends in resistance during the partial dehydration step were observed for Ag-hydrogel composites with different Ag contents (Supplementary Figure 5c-f). As the initial Ag content increased, the exponential decrease in resistance occurred more quickly, demonstrating the effect of drying on the electrical conductivity.

Importantly, the percolation network appears to be permanently formed as a result of the dehydration step. When the resistance was recorded in an aqueous environment where it could rehydrate (Supplementary Figure 6), the Ag-hydrogel composite maintained high electrical conductivity. The resistance was observed to increase after three days in water due to swelling of the hydrogel matrix. However, the percolating network remained largely intact and the absolute resistance was on the same order of magnitude as prior to rehydration. The absorbed water imposed capillary force that disrupted weak conductive pathways of Ag flakes. However, the main percolating network remained due to the comparatively stronger adhesion between contacting flakes (Supplementary Discussion 1 and Supplementary Figure 7 and 8). In this way, the material was still able to show high electrical conductivity even after being submerged in an aqueous environment for three days (Supplementary Figure 6 and 9). The results could be compared to an Ag-hydrogel composite that was left in ambient air after partial dehydration, where the resistance decreased slightly (Supplementary Figure 6). These results highlight the importance of controlled assembly by dehydration to fabricate the soft conductor.

High electrical conductivity enables the Ag-hydrogel composite to deliver high direct current at low voltages. We first applied a constant voltage and monitored direct current over time for a printed Ag-hydrogel trace which became electrically conductive after the partial dehydration process (Supplementary

Figure 10a). Voltages were applied to give initial current values (I_0) of 1, 2, 3, and 4 A, and the corresponding normalized resistance was also monitored over time (Fig. 2b). For lower currents (I_0 = 1 or 2 A), the resistance profiles are stable, which demonstrates the electrical stability of the Ag-hydrogel. The resistance gradually decreased when subjected to an initial current of 3 A. When initial direct current of 4 A was applied, we observed a substantial decrease of resistance within 10 minutes. The decreased resistance saturated at the end of the test. We attribute this resistance decrease to further evaporation of water (beyond the intentional partial dehydration) between adjacent Ag flakes as the composite was heated by Joule heating at high current.

Finite element analysis (FEA) of Joule heating at steady-state and the long-term response to high current were compared. The results of simulation (Supplementary Figure 10c-f) and long-term response to high current (Supplementary Figure 11) show that the maximum temperature exceeds the boiling point of water (100 °C) when the composite is subjected to an electrical power with an initial current of 3 A and 4 A. This localized high temperature produces bubbles (Supplementary Figure 12g-l) near the Ag-hydrogel trace and can result in thermal degradation of the hydrogel at 4 A (i.e., the discoloration of the hydrogel as shown in Supplementary Figure 12j-l and Supplementary Figure 13). In contrast, Ag-hydrogel traces subjected to lower electrical currents (I_0 = 1 and 2 A) retain their original appearance (e.g., minimal bubbles and no discoloration) due to the lower localized temperature (<100 °C, Supplementary Figure 10c-d and 11c-d). We further investigated the long-term response of the Ag-hydrogel composite to direct current while underwater. The results in Supplementary Figure 14 show that the Ag-hydrogel can maintain high electrical conductivity in an aqueous environment during long-term usage (Supplementary Discussion 2). These results demonstrate the potential of the Ag-hydrogel composite as a power line for applications in digital electronics that require high direct current and can retain functionality in various environments.

To be mechanically compatible with soft biological tissues, the Ag-hydrogel composite must be highly compliant and deformable. The stress-strain characteristics were evaluated using an Instron 5969 materials testing machine (Fig. 2c). We calculated the effective elastic modulus (Fig. 2c inset) by adopting the hyperelastic constitutive model for a 2-parameter Ogden solid[46] and performing a statistical fit (R-squared = 0.95). The 5 vol% Ag-hydrogel composite has a modulus of 5-6 kPa after performing partial dehydration (Supplementary Figure 15), while the unfilled PAAm-alginate hydrogel's modulus is about 3-4 kPa. As observed with other conductive composites[16,40], the introduction of metallic fillers into a soft matrix typically results in a composite with higher Young's modulus than that of an unfilled matrix. However, since the Ag content is kept low by controlling assembly through the partial dehydration, the Ag-hydrogel composite has tissue-like softness and minimal hysteresis between mechanical loading and unloading.

Conductors that interface with biological tissues typically undergo complex and repetitive deformations and so it is crucial to understand the electromechanical coupling of the soft conductor. Electromechanical coupling of the Ag-hydrogel was measured by monitoring the change in resistance of a stencil-printed composite trace as a function of uniaxial strain. The printed composite was encapsulated with another layer of PAAm-alginate hydrogel after the partial dehydration to prevent further dehydration (see Methods). We first examined changes in electrical resistance while subsequently imposing different tensile strains (ε = 50, 100, 150, 200, and 250%; Fig. 2d). The Ag-hydrogel was first stretched by 50% strain and then relaxed to its original length, and the strain was increased by 50% up to 250% for each successive cycle. The stretching and releasing curves overlapped, highlighting negligible hysteresis in resistance under different mechanical loading conditions. Since the conductive hydrogel composite shows small mechanical hysteresis, the resistance of the composite also shows small changes under cyclic loadings (Supplementary Figure 16). In addition, the resistance change at small strain (0~100%) agrees well with Pouillet's law[47], i.e., $\Delta R/R_0 = (1+\varepsilon)^2 - 1$, where ε is strain, R is resistance, and R_0 is the initial resistance at small strain (0~100%). Moreover, these tests demonstrate that the Ag-hydrogel is highly stretchable while maintaining electrical conductivity at strains up to 250%.

Importantly, the composite should be electromechanically robust to multiple strain cycles. Through multiple strain cycles between 0% and 100% strain, the resistance of the Ag-hydrogel remains low enough for practical purposes, such as digital circuit functionality or bioelectronics (Fig. 2e). Through 10 cycles, the resistance remained relatively constant, with less than 1 Ω change in the relaxed state. When stretched, the electromechanical response was fast, changing according to the mechanical deformation within 0.1 seconds (Supplementary Figure 16b-c). While being held right after stretching for 20 seconds, the resistance exponentially drops at first and the changes in resistance are about 1.2 Ω which are consistent throughout the 10 cycles. These experiments illustrate the desirable electromechanical features of the Ag-hydrogel, which include fast electrical response (20~40 ms when stretched and 160~250 ms when released) to external mechanical stimuli and a robust percolating network for repeatable and consistent elastic response.

To validate long-term use, the Ag-hydrogel was also characterized for 1,000 cycles of tensile loading between 0% and 100% strain (Fig. 2f). The resistance at 0% and 100% strain was bounded within stable boundaries for the first one hundred cycles, then slightly increased from 2.5 Ω to 4.2 Ω at 0% strain and from 10 Ω to 16 Ω at 100% strain. For subsequent loading cycles, the resistance of the conductive hydrogel composite at 100% strain was observed to increase and then fluctuate when approaching 1,000 cycles. The reason for this fluctuation was that the experiment was conducted in air with a relatively rapid speed of 10 mm s^{-1}, which led the sample to become drier and stiffer over the duration of the experiment (100 mins). This could be avoided by performing the experiment in a humid environment. Nonetheless, the

results of electromechanical characterization demonstrate the composite's high conductivity, low electromechanical hysteresis, and repeatable electrical response to mechanical deformation.
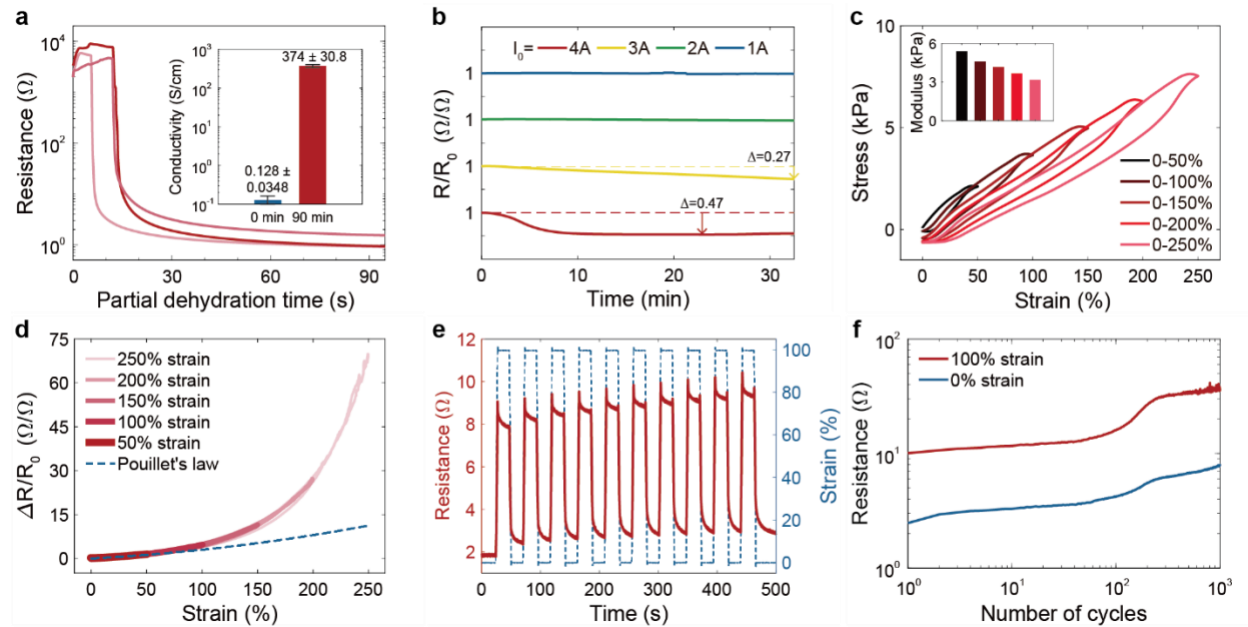

Fig. 2 | Material characterization. a, Absolute change in resistance as a function of time for partial dehydration process and (inset) the volumetric conductivity at 0 min and 90 min. The error bars are the standard deviation for $N = 3$ samples. This is for a composite with an initial Ag content of 5 vol%; plots for composites with other initial volume fractions are presented in Supplementary Figure 5. **b**, Normalized change in resistance as a function of time with different initial currents and corresponding constant voltages; note, the y axis offset is applied to each curve to assist in visualization of the data. Here, Δ is defined as the change of R/R_0 compared to its initial value of 1. **c**, Stress versus strain of the conductive hydrogel composite under different uniaxial loading conditions from 0% to 50%, 100%, 150%, 200%, and 250% strain, and effective elastic moduli as a function of loading condition (inset). **d**, Normalized change in resistance as a function of strain (gradient of red solid lines) along with the theoretical prediction using Pouillet's law for an incompressible elastomer with constant volumetric resistivity (dashed blue line). **e**, Electromechanical response as a function of time under uniaxial cyclic loading to 100% strain up to the first 10 cycles. For each cycle, the sample was stretched at 10 mm s^{-1}, held for 20 seconds, released at 10 mm s^{-1}, and held for 20 seconds. **f**, Cycling stability of the resistance under uniaxial cyclic loading to 100% strain up to 1,000 cycles. The sample was stretched and released at the speed of 10 mm s^{-1}.

Stingray-inspired soft swimmer

The tissue-like compliance and deformability of the Ag-hydrogel composite – along with its electrical conductivity – permit its use as a soft conductive material in soft robotics. To demonstrate its potential in soft robotics, we fabricated a stingray-inspired soft swimmer that was composed of a pair of hydrogel pectoral fins and a streamlined backbone made with a soft foam. Two sets of Ag-hydrogel traces formed compatible interfaces with the hydrogel pectoral fins. The soft and conductive traces served as power lines to deliver high current (~3.3A) from a benchtop power supply (KPS3010D, Eventek) to a pair of shape memory alloy (SMA) actuators without interfering with the natural deformability and compliance of the hydrogel pectoral fin (Fig. 3a). The soft actuators were composed of two SMA wires sandwiched by three layers of VHB tapes (4905, 3M), which enabled the actuators to bend upward and downward alternatively through direct Joule heating[48] (see Methods). To induce a forward swimming motion, the top pair of SMA wires were activated for 0.6 seconds and then cooled for 1.9 seconds while the other pair were activated and cooled for 0.3 and 2.2 seconds, respectively (Fig. 3b and 3c). Referring to Fig. 3c, the upward and downward actuation cycles were staggered with a 0.9 second offset period. The stingray-inspired swimmer is capable of swimming at an average speed of 0.2 body lengths per second (40 mm s^{-1}) (Fig. 3d; Supplementary Movie 2). This demonstration highlights the electrical conductivity and stability of the Ag-hydrogel by carrying high currents (3.3 A) to activate the embedded SMA actuators.
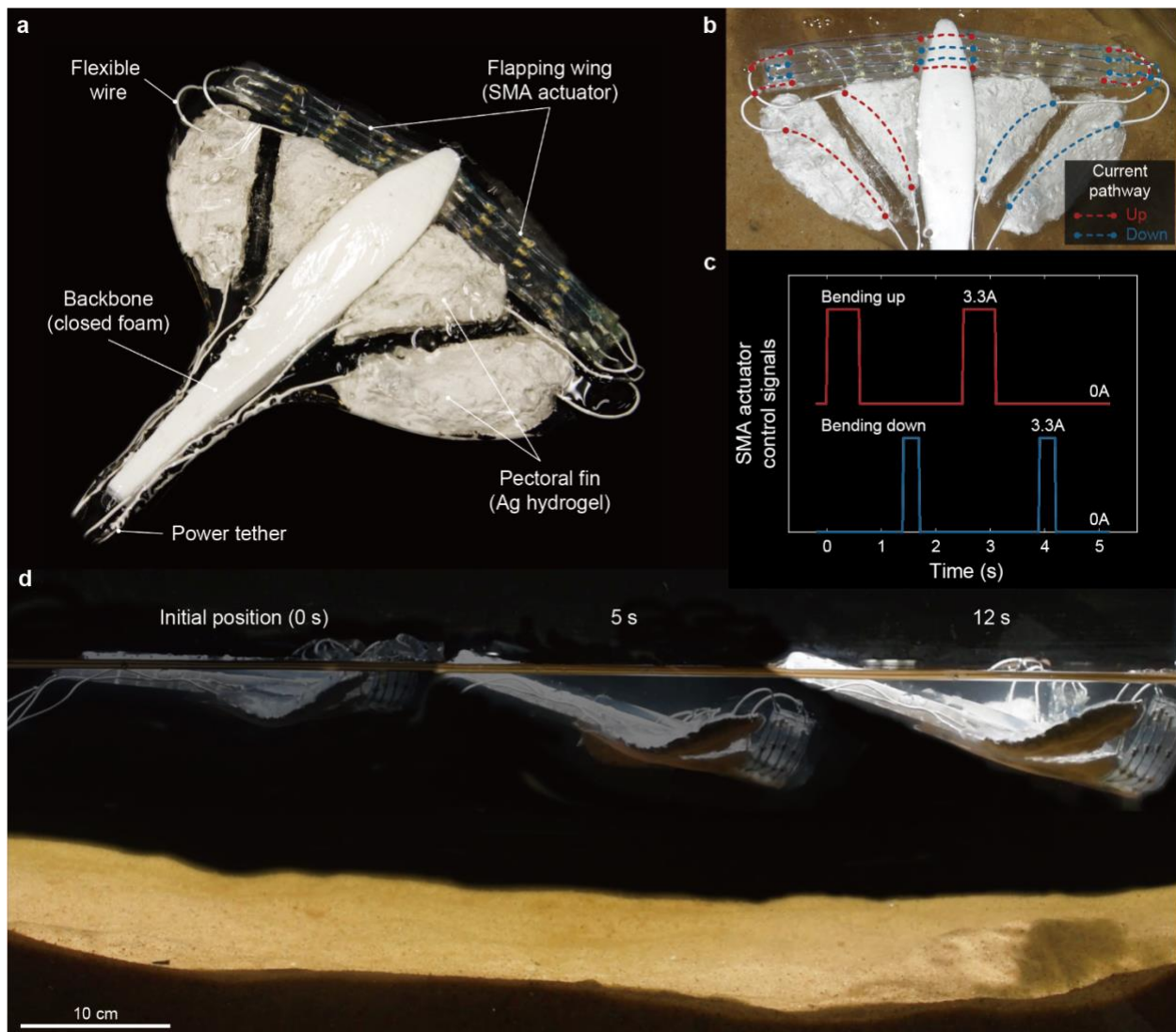
Fig. 3 | Stingray-inspired soft swimmer. a, A soft stingray-inspired swimmer with the conductive hydrogel composite. The soft swimmer is propelled by shape-memory alloy (SMA) wires, which require high current (3.3 A) to be actuated and are connected to the tethered power through the conductive hydrogel composite. **b,** Schematic of high-current signal routing, connecting the SMA wires and the power; the trace is color-coded with reference to **c. c,** Actuation sequence and required current for the soft swimmer. **d,** Sequential images of the soft swimmer from the side view (Supplementary Movie 2).

Neuromuscular electrical stimulation electrode

The soft and highly conductive Ag-hydrogel composite also has the potential to broaden the utilization of hydrogels as electrodes in the field of epidermal electrical stimulation and recording, which requires electrodes with adequate electrical conductivity[21,49]. Here, we fabricated Ag-hydrogel electrodes to deliver high frequency electrical signals for neuromuscular electrical stimulation (NMES)[50] to demonstrate the enabling bioelectronic properties of the composite. As shown in Fig. 4a, a pair of Ag-hydrogel electrodes is connected to a commercial electrical muscle stimulator (PowerDot 2.0 Uno, PowerDot), where the strength and frequency of the pulses are controllable using a smartphone via Bluetooth. For comparison, we also made unfilled hydrogel electrodes with ionic conductivity and performed NMES under the same conditions (see Methods and Supplementary Figure 17). First, the electrodes stimulate the tibialis anterior muscle of the leg, which dorsiflexes the foot when stimulated (Fig. 4b and Supplementary Video 3). With the same stimulation intensity, we measured the relative change in dorsiflexion angle from the side view (Fig. 4c) and the frequency of vibration (Fig. 4d). Fig. 4d shows that the frequencies of muscle stimulation in both cases are almost identical because the signal was generated by the same device and power. However, as shown in Fig. 4c, the relative changes in dorsiflexion angle are different in both cases: the Ag-hydrogel electrodes were able to deliver sufficient current to induce dorsiflexion in foot, whereas the electrodes made of ionic hydrogel appeared ineffective to conduct enough current to contract the muscle. We also compared the performance of the Ag-hydrogel electrodes and commercial electrodes (made by PowerDot) along with the NMES device, which shows that the Ag-hydrogel electrodes have comparable performance to the commercially available NMES electrodes (Supplementary Figure 18). The next experiment was conducted on the muscles in the posterior of the forearm, which results in tremors in the wrist and the fingers curling in towards the palm (Fig. 4e, Supplementary Figure 17, and Supplementary Video 4). The result shows that the stimulation driven by Ag-hydrogel electrodes exhibits more significant angle change between the proximal phalange and the metacarpus of the ring and little finger compared to the case of ionic hydrogel electrodes. This demonstration suggests that the Ag-hydrogel composite has the potential to improve bioelectronic interfacing of tissue-electrode contacts due to its high electrical conductivity and soft conformability.
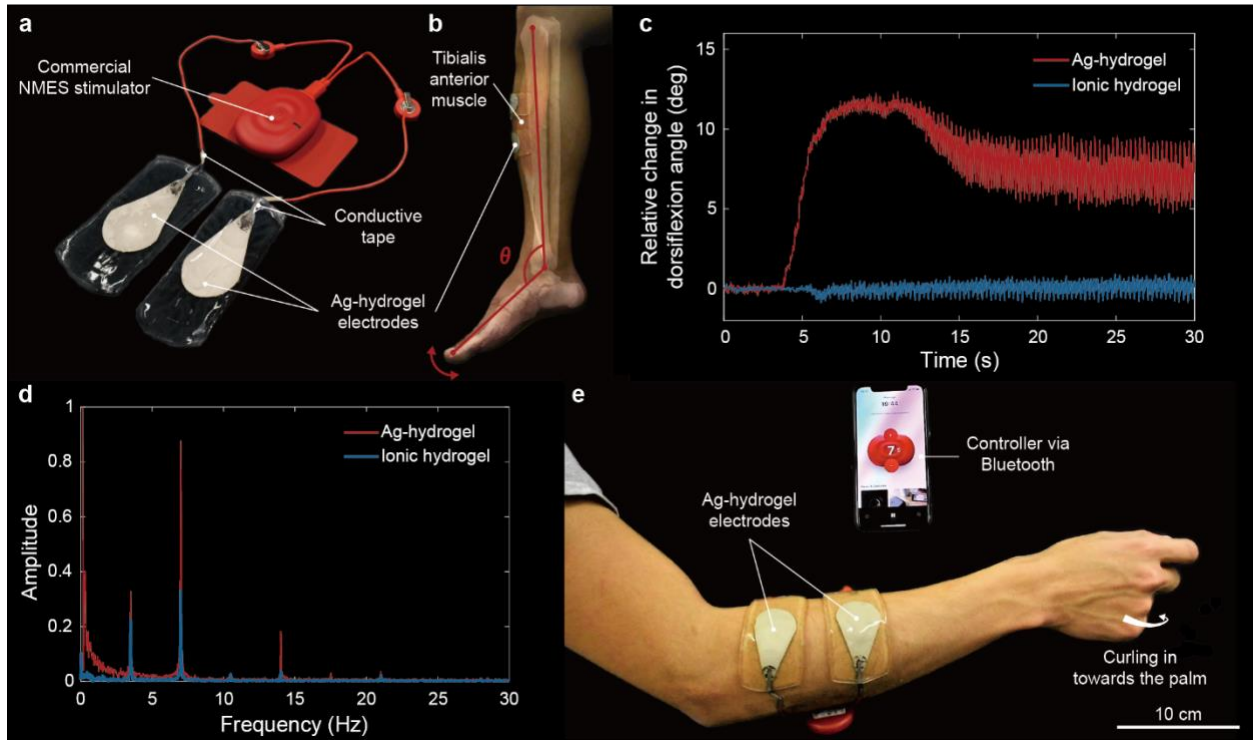
Fig. 4 | Neuromuscular electrical stimulation (NMES) electrode. a, NMES electrodes made of the Ag-hydrogel composite are assembled with a commercial electrical muscle stimulator. **b**, The electrodes are placed on the tibialis anterior muscle of the subject's leg to cause dorsiflexion (Supplementary Video 3). The red lines are used to track the relative change of the angle (θ) which is measured in **c**. **c**, Relative change in dorsiflexion angle as a function of stimulation time. **d**, Amplitude as a function of frequency, which is the result of fast Fourier Transform (FFT). **e**, The electrodes are placed on the arm and delivering electrical signals from the stimulator to the muscles in the posterior of the forearm (Supplementary Video 4).

Conclusions

We have reported an Ag-hydrogel composite that is based on two materials with disparate mechanical properties – Ag flakes and hydrogel matrix – and exhibits high electrical conductivity (>300 S cm^{-1}), electrical stability under repeated mechanical loading, low Young's modulus (<10 kPa), and high stretchability (up to 250% strain without electrical failure). To illustrate the capabilities of the Ag-hydrogel, we fabricated a stingray-inspired swimmer driven by SMAs that require high current, high compliance, and high stretchability for actuation. We also developed skin-mounted electrodes made of the Ag-hydrogel for neuromuscular electrical stimulation, which require conformal contact and high conductivity in order to deliver electrical impulse with high frequency.

This combination of both high electrical conductivity and high compliance is achieved by controlling the assembly of Ag inclusions when dispersing the micron-sized Ag flakes in the polyacrylamide and alginate hydrogel. A key step in the fabrication process is the partial dehydration step, which allows intimate contact between Ag flakes and the formation of a percolating network that remains intact and stable even as the gel is fully rehydrated. The conductive hydrogel composites also have robust and reliable electromechanical coupling, which facilitates applications in soft robotic systems, wearable electronics, and bioelectronic interfacing. The combination of electrical and mechanical properties of the Ag-hydrogel composite occupies a unique place in the design space of electrically conductive soft materials (Fig. 1c and Supplementary Figure 1) and could be of use in the development of soft robotics, bioelectronics, and wearable electronics.

Methods

Materials. The chemical used as components of the hydrogel were dissolved in deionized water (McMaster-Carr). For polyacrylamide (PAAm) gel, 40 wt% acrylamide (AAm, A8887; Sigma-Aldrich) was used as the monomer for the polyacrylamide hydrogel network. 1 wt% of *N*, *N*-methylenebisacrylamide (MBAA, 146072; Sigma-Aldrich) was used as the crosslinker. 5 wt% of ammonium persulphate (APS, A3678; Sigma-Aldrich) was used for curing hydrogel substrates and 20 wt% of APS was used for curing Ag-hydrogel composites. In both cases, APS functions as thermal or photo initiator. 5 wt% of *N, N, N', N'*-tetramethylethylenediamine (TEMED, T9281; Sigma-Aldrich) was used as accelerator to make the curing process faster. For alginate gel, sodium alginate (W201502; Sigma-Aldrich) was used as the monomer for the alginate hydrogel network. For conductive fillers, micron-scale sized Ag flakes (2-5 µm, 47MR-10F; Inframat Advanced Materials, LLC) were mixed with the PAAm-alginate hydrogel matrix.

Synthesis of PAAm-alginate hydrogel. We synthesized stretchable and tough hydrogels by mixing linear copolymer alginate and covalently crosslinked polyacrylamide using a method adopted from previous works[43,51]. Unless otherwise stated, the water content of hydrogel was fixed at 86 wt% when the hydrogel is initially cured. We mixed alginate with 40 wt% AAm in water solution with additional deionized water and waited until alginate was fully dissolved. The ratio of alginate to AAm was 1:6 by weight. When alginate became fully dissolved, the mixture was mixed with 1 wt% MBAA (0.06% of the total weight of AAm) and 5 wt% TEMED (0.24% of the total weight of AAm). For the last step of synthesizing process, 5 wt% APS (0.75% of the total weight of AAm) was added to cure the hydrogel pre-gel solution. The chemicals used in this process were mixed by using a planetary centrifugal mixer at 2000 rpm (AR-100; Thinky Corporation).

Synthesis of conductive Ag-hydrogel composite. We synthesized a conductive hydrogel composite by mixing the abovementioned PAAm-alginate hydrogel with micron-sized Ag flakes. Ag flakes (5 vol% of the volume of hydrogel) were mixed with the mixture of alginate, deionized water, and 40 wt% AAm. The mixture was mixed once more after adding MBAA and TEMED. However, with the same amount of chemical components as the case of PAAm-alginate hydrogel, the mixture was not cured because of the dispersed Ag flakes within the hydrogel pre-gel solution. By increasing the amount of 1 wt% MBAA by a factor of five (corresponding to 0.3% of the total weight of AAm), the crosslinking network between polymer chains was successfully formed in the presence of Ag flakes. Additionally, to increase the curing rate, 20 wt% APS (3% of the total weight of AAm) was used.

Partial dehydration process. We used a digital multimeter (34401A; Keysight Technologies or 2100; Keithley, Supplementary Figure 19) with a four-point probe to record the change in resistance of the printed Ag-hydrogel composite (40 mm length, 3 mm width, and 0.7 mm thickness) on a 1.6 mm thick PAAm-alginate hydrogel substrate. EGaIn (Eutectic Gallium-Indium, mixture 75 wt% Gallium and 25 wt% Indium; Solution Materials, LLC) was used at each end of printed trace to minimize contact resistance between probes and conductive hydrogel composite. The partial dehydration process proceeded in an acrylic box with some holes, where humidity and temperature of the environment in the box were monitored by a digital sensor (B07HMV6GG2, Linkstyle). The resistance values were manually recorded. These tests were conducted in a lab room with an air conditioner that set the room temperature around 22 °C.

Volumetric conductivity. The volumetric conductivity ($\sigma = l/RA$) of the printed Ag-hydrogel trace was calculated using an effective trace length ($l=40$ mm) and effective cross-sectional area ($A=1.76$ μm^2 for the case before partial dehydration process and $A=1.38$ mm^2 for the case after partial dehydration process; see Supplementary Figure 5 for a representative sample dimensions). The cross-sectional area was measured using a digital microscope (1000X; MicroTroniX).

Electro-mechanical characterization. Ag-hydrogel composite was stencil-printed on a 1.6 mm thick PAAm-alginate hydrogel. EGaIn was located at each end of the printed trace to minimize contact resistance between conductive hydrogel composite and wires from an USB DAQ (USB-6002; NI), which collects

external analogue data from the materials testing machine (5969; Instron) at a rate of 1 kHz. After partial dehydration process was completed, the printed Ag-hydrogel composite was sealed by pre-gel PAAm-alginate hydrogel when the resistance reached 2 Ω. In 10 mins, the pre-gel solution started to be cured. The samples were cut around the trace by a razor blade and assembled with 3d printed grips. The data was saved using a software (MATLAB, 2016a) that can communicate with the USB DAQ.

Electrical stability test. Samples were prepared in the same way of the samples used in electro-mechanical tests; a printed Ag-hydrogel composite trace within two layers of 1.6 mm thick PAAm-alginate hydrogel. The samples were directly connected to a benchtop power supply (KPS3010D; Eventek). The power supply was set to supply fixed voltage to generate pre-defined initial direct current (1, 2, 3, or 4 A). The current values were manually recorded.

FEA simulation of Joule heating. Composites were simulated using SOLIDWORKS (Dessault Systèmes). The geometry of an Ag-hydrogel trace was set as 40 mm × 3 mm × 0.7 mm. The Ag-hydrogel was encapsulated between two layers of PAAm-alginate hydrogel with a diameter of 83 mm and a thickness of 1.6 mm. The FEA simulation was conducted using Ansys Thermal-Electric toolbox. We set the thermal conductivity of the hydrogel layer and Ag-hydrogel trace at 1.045 W $(m·°C)^{-1}$ [52] and 25.62 W $(m·°C)^{-1}$ [53], respectively. Additionally, we used $3.086 × 10^{-3}$ Ω·cm for the Ag-hydrogel composite's resistivity and 20 Ω·cm[54] for the PAAm-algiante hydrogel's resistivity. Then, two conditions were applied to the model: (1) voltage conditions and (2) convection conditions. For voltage conditions, a fixed voltage difference was applied to the end of the Ag-hydrogel trace. The value was varied by each case. For convection conditions, we used 'Stagnant Air - Simplified Case' at 22 °C with a heat transfer coefficient of 5 W $(m^2·°C)^{-1}$. This condition is applied to the top surface of the additional layer of PAAm-alginate hydrogel and to the sides of the sample. We also set a constant temperature of 22 °C on the bottom of the sample as a boundary condition.

Mechanical characterization. Samples were prepared in a dogbone shape (Die A, ASTM D412) and tested on a materials testing machine (5969; Instron) at a strain rate of 20 mm min^{-1}, unless otherwise stated. Each sample was cured in a 5 mm thick polyacrylate mould that was printed using a 3d printer (Objet24; Stratasys, Ltd). After fabrication (see the Synthesis section), samples were clamped by self-tightening roller grips (2713-001; Instron). Total two different types of samples were tested: (i) PAAm-alginate hydrogel without conductive fillers and (ii) Ag-hydrogel composite.

Environmental stability test. Samples were prepared in the same way of the samples used in electro-mechanical tests and electrical stability tests. The resistance of the trace was measured using a digital multimeter (34420A; HP) with a four-point probe. The data was collected using a script in MATLAB (2016a, MathWorks). For the ambient air experiment, the samples were left unattended without any additional treatment for 3 days. Otherwise, for the water experiment, the samples were contained in glass beakers. After initial setup to measure the resistance, deionized water was added to submerge the trace using a disposable plastic pipette. For 3 days, deionized water was properly resupplied to keep the aqueous environment.

Stingray-inspired soft swimmer fabrication. We started fabrication of the stingray-inspired swimmer by laser-cutting the soft closed foam into a streamlined shape. Then we cut a rectangular through-hole on the side of the streamlined body so that the actuators can be inserted through it. The actuator was composed of four nitinol wires (0.38 mm in diameter; Dynalloy, Inc.) that were trained to curled shapes by fixing them on aluminium cylinder moulds and baking in an oven for 25 minutes at 500 °C along with a quenching process. Each pair of two trained nitinol wires was connected with a small piece of ultra-flexible wire (9564T1; McMaster-Carr) and placed on the top of a rectangular VHB tape (80×20×0.5 mm, 4905; 3M) with the bending direction facing downward. Next, the nitinol wires with the VHB tapes were placed on both sides of a rectangular VHB tape with the same dimension. After the assembly, the actuator was capable of bending both upwards and downwards by direct Joule heating. After that, we connected two actuators

with the ultra-flexible wires and nitinol wires with the same bending direction were connected in series. The actuators were inserted through the rectangular hole on the backbone with the identical length and angle extruded (Supplementary Figure 20a). Finally, the backbone and the actuators were placed in a 3d printed mould that was lined with a cured thin layer of PAAm-alginate hydrogel. The Ag-hydrogel composite was stencil-printed into the shape of pectoral fins along the outline of the mould (Supplementary Figure 20b). At the end of each line of the conductive hydrogel, ultra-flexible wire was embedded and connected to the wire of the SMA actuators. The other end of the flexible wire was soldered with another long wire to connect with an external control board. When the Ag-hydrogel achieved certain conductivity (see Partial dehydration process), additional pre-gel PAAm-alginate hydrogel was poured on top of the assembled components. After the additional hydrogel was cured, the swimmer was then gently detached out of the mould in an aqueous environment.

Neuromuscular electrical stimulation electrode fabrication. We made two versions of NMES electrodes: electrodes made of the electrically conductive Ag-hydrogel and electrodes made of ionically conductive PAAm-alginate hydrogel. First, we made a 1.6 mm thick PAAm-alginate hydrogel substrate. When the substrate was crosslinked, the conductive tape was placed on the substate as a bridge between a commercial neuromuscular electrical stimulator (PowerDot). Thin layer of EGaIn was deposited on the conductive tape as a soft conductor to minimize the contact resistance. For the case of electrodes of Ag-hydrogel, the conductive hydrogel composite was stencil-printed on top of the substrate and the conductive tape. After that, pre-gel solution of PAAm-alginate hydrogel was poured at the very top as the second layer of electrodes. At this step, for the version of conductive hydrogel composite, a certain amount of time was required to wait for the material to be electrically conductive. The electrode can be cut into desirable form factors for specific muscle using a razor blade (Supplementary Fig. 17a). To connect the electrodes to the stimulator, each electrode was soldered with a wire that electrically connected with a magnet at the end of it (Fig. 4a). The electrodes and the stimulator can be connected though the magnet without compromising the electrical properties. The authors obtained research participants consent beforehand.

Motion analysis of neuromuscular electrical stimulation. To quantify the response of muscle stimulation, videos were recorded using a Nikon D5600 camera at a frame rate of 60 Hz. For the lower-limb stimulation videos, we developed a customized tracking algorithm to locate the end points of the tibia and the toe in every frame by template matching of skin features in order to calculate the dorsiflexion angle. The reference line of the tibia is defined by its two end points, whereas the reference line of the foot is defined by the lower end point of tibia and the toe, assuming flexion of the latter is negligible. The reference lines were used to calculate the change in dorsiflexion angle relative to its initial position, taken as the average from the first second. The two videos with Ag-hydrogel and ionic hydrogel are synchronized by the starting point of the PowerDot stimulation program.

Data availability. The datasets generated during and/or analysed during the current study are available from the corresponding author on reasonable request.

References

1. Lin, S. *et al.* Stretchable Hydrogel electronics and devices. *Adv. Mater.* **28**, 4497-4505 (2015).
2. Schiavone, G. *et al.* Soft, implantable bioelectronic interfaces for translational research. *Adv. Mater.* **32**, 1906512 (2020).
3. Pan, L. *et al.* Hierarchical nanostructured conducting polymer hydrogel with high electrochemical activity. *Proc. Natl. Acad. of Sci. U.S.A.* **109**, 9287-9292 (2012).
4. Dejace, L., Laubeuf, N., Furfaro, I. & Lacour, S. P. Gallium-based thin films for wearable human motion sensors. *Adv. Intell. Syst.* **1**, 1900079 (2019).
5. Qiu, T., Palagi, S., Sachs, J. & Fischer, P. Soft miniaturized linear actuators wirelessly powered by rotating permanent magnets. *Proceedings - IEEE International Conference on Robotics and Automation* (2018).
6. Zhang, W., Feng, P., Chen, J., Sun, Z. & Zhao, B. Electrically conductive hydrogels for flexible energy storage systems. *Prog. Polym. Sci.* **88**, 220-240 (2019).
7. Shi, Y. & Yu, G. Designing hierarchically nanostructured conductive polymer gels for electrochemical energy storage and conversion. *Chem. Mater.* **28**, 2466-2477 (2016).
8. Larson, C. *et al.* Highly stretchable electroluminescent skin for optical signalling and tactile sensing. *Science* **351**, 1071-1074 (2016).
9. Kim, C.-C., Lee, H.-H., Oh, K. H. & Sun, J.-Y. Highly stretchable, transparent ionic touch panel. *Science* **353**, 682-687 (2016).
10. Kim, J. *et al.* Battery-free, stretchable optoelectronic systems for wireless optical characterization of the skin. *Sci. Adv.* **2**, e1600418 (2016).
11. Lee, W. *et al.* Integration of organic electrochemical and field-effect transistors for ultraflexible, high temporal resolution electrophysiology arrays. *Adv. Mater.* **28**, 9722-9728 (2016).
12. Lin, Y. *et al.* Vacuum filling of complex microchannels with liquid metal. *Lab Chip* **17**, 3043-3050 (2017).
13. Koh, A. *et al.* A soft, wearable microfluidic device for the capture, storage, and colorimetric sensing of sweat. *Sci. Transl. Med.* **8**, 366ra165 (2016).
14. Pan, C. *et al.* Silver-coated poly(dimethylsiloxane) beads for soft, stretchable, and thermally stable conductive elastomer composites. *ACS Appl. Mater. Interfaces* **11**, 42561-42570 (2019).
15. Tavakoli, M. *et al.* EGaIn-assisted room-temperature sintering of silver nanoparticles for stretchable, inkjet-printed, thin-film electronics. *Adv. Mater.* **30**, 1801852 (2018).
16. Wang, J. *et al.* Printable superelastic conductors with extreme stretchability and robust cycling endurance enabled by liquid-metal particles. *Adv. Mater.* **30**, 1706157 (2018).
17. Markvicka, E. J., Barlett, M. D., Huang, X. & Majidi, C. An autonomously electrically self-healing liquid metal–elastomer composite for robust soft-matter robotics and electronics. *Nat. Mater.* **17**, 618-624 (2018).
18. Fassler, A. & Majidi, C. Liquid-phase metal inclusions for a conductive polymer composite. *Adv. Mater.* **27**, 1928-1932 (2015).
19. Comley, K. & Fleck, N. A. A micromechanical model for the Young's modulus of adipose tissue. *Int. J. Solids Struct.* **47**, 2982-2990 (2010).
20. Keplinger, C. *et al.* Stretchable, transparent, ionic conductors. *Science* **341**, 984-987 (2013).
21. Yuk, H., Lu, B. & Zhao, X. Hydrogel bioelectronics. *Chem. Soc. Rev.* **48**, 1642-1667 (2019).
22. Kim, D.-H. *et al.* Epidermal electronics. *Science* **333**, 838-843 (2011).
23. Kim, D.-H. *et al.* Dissolvable films of silk fibroin for ultrathin conformal bio-integrated electronics. *Nat. Mater.* **9**, 511-517 (2010).
24. Minev, I. R. *et al.* Electronic dura mater for long-term multimodal neural interfaces. *Science* **347**, 159–163 (2015).
25. Xu, L. *et al.* 3D multifunctional integumentary membranes for spatiotemporal cardiac measurements and stimulation across the entire epicardium. *Nat. Commun.* **5**, 3329 (2014).
26. Erol, O., Pantula, A., Liu, W. & Gracias, D. H. Transformer hydrogels: A review. *Adv. Mater. Technol.* **4**, 1900043 (2019).
27. Han, L. *et al.* A mussel-inspired conductive, self-Adhesive, and self-healable tough hydrogel as cell stimulators and implantable bioelectronics. *Small* **13**, 1601916 (2016).
28. Palagi, S. *et al.* Structured light enables biomimetic swimming and versatile locomotion of photoresponsive soft microrobots. *Nat. Mater.* **15**, 647-653 (2016).
29. Lopes, P. A. *et al.* Soft bioelectronic stickers: selection and evaluation of skin-interfacing electrodes. *Adv. Healthc. Mater.* **8**, 1900234 (2019).
30. Yuk, H. *et al.* Hydraulic hydrogel actuators and robots optically and sonically camouflaged in water. *Nat.*

Commun. **8**, 14230 (2017).

31. Yang, C. & Suo, Z. Hydrogel ionotronics. *Nat. Rev. Mater.* **3**, 125-142 (2018).

32. Lee, H.-R., Kim, C.-C. & Sun, J.-Y. Stretchable ionics - A promising candidate for upcoming wearable devices. *Adv. Mater.* **30**, 1704403 (2018).

33. Rivnay, J., Wang, H., Fenno, L., Deisseroth, K. & Malliaras, G. G. Next-generation probes, particles, and proteins for neural interfacing. *Sci. Adv.* **3**, e1601649 (2017).

34. Lu, B. *et al.* Pure PEDOT:PSS hydrogels. *Nat. Commun.* **10**, 1043 (2019).

35. Dvir, T. *et al.* Nanowired three-dimensional cardiac patches. *Nat. Nanotechnol.* **6**, 720-725 (2011).

36. Ahn, Y., Lee, H., Lee, D. & Lee, Y. Highly conductive and flexible silver nanowire-based microelectrodes on biocompatible hydrogel. *ACS Appl. Mater. Interfaces* **6**, 18401-18407 (2014).

37. Lim, C. *et al.* Stretchable conductive nanocomposite based on alginate hydrogel and silver nanowires for wearable electronics. *APL Mater.* **7**, 031502 (2019).

38. Jing, X. *et al.* Stretchable gelatin/silver nanowires composite hydrogels for detecting human motion. *Mater. Lett.* **237**, 53-56 (2019).

39. Shin, S. R. *et al.* Carbon-nanotube-embedded hydrogel sheets for engineering cardiac constructs and bioactuators. *ACS Nano* **7**, 2369-2380 (2013).

40. Jo, H. *et al.* Electrically conductive graphene/polyacrylamide hydrogels produced by mild chemical reduction for enhanced myoblast growth and differentiation. *Acta Biomater.* **48**, 100-109 (2017).

41. Zhao, W., Han, Z., Ma, L., Sun, S. & Zhao, C. Highly hemo-compatible, mechanically strong, and conductive dual cross-linked polymer hydrogels. *J. of Mater. Chem. B* **4**, 8016-8024 (2016).

42. Feig V. R. *et al.* Mechanically tunable conductive interpenetrating network hydrogels that mimic the elastic moduli of biological tissue. *Nat. Commun.* **9**, 2740 (2018).

43. Sun, J.-Y. *et al.* Highly stretchable and tough hydrogels. *Nature* **489**, 133-136 (2012).

44. Yang, C. H. *et al.* Strengthening alginate/polyacrylamide hydrogels using various multivalent cations, *ACS Appl. Mater. Interfaces* **5**, 10418-10422 (2013).

45. Mondal, S., Das, S. & Nandi, A. K. A review on recent advances in polymer and peptide hydrogels. *Soft Matter* **16**, 1404-1454 (2020).

46. Ogden, R. W. Large deformation isotropic elasticity−On the correlation of theory and experiment for incompressible rubberlike solids. *Rubber Chem. Technol.* **46**, 398-416 (1973).

47. Kim, H. J., Son, C. & Ziaie, B. A multiaxial stretchable interconnect using liquid-alloy-filled elastomeric microchannels. *Appl. Phys. Lett.* **92**, 1-4 (2008).

48. Huang, X., Kumar, K., Jawed, M. K., Ye, Z. & Majidi, C. Soft electrically actuated quadruped (SEAQ)-integrating a flex circuit board and elastomeric limbs for versatile mobility. *IEEE Robot. Autom. Lett.* **4**, 2415-2422 (2019).

49. Li, H., Erbaş, A., Zwanikken, J. & Cruz, M. O. D. L. Ionic conductivity in polyelectrolyte hydrogels. *Macromolecules* **49**, 9239-9246 (2016).

50. Lake, D. A. Neuromuscular Electrical Stimulation. *Sport. Med.* **13**, 320-336 (1992).

51. Yuk, H., Zhang, T., Lin, S., Parada, G. A. & Zhao, X. Tough bonding of hydrogels to diverse non-porous surfaces. *Nat. Mater.* **15**, 190-196 (2016).

52. Xu, S., Cai, S., Liu, Z. Thermal conductivity of polyacrylamide hydrogels at the nanoscale. *ACS Appl. Mater. Interfaces* **10**, 36352-36360 (2018).

53. Hugh, D. Y. & Freedman, R. A. *University physics*. (Addison-Wesley, 1992).

54. Thibodeau, J. & Ignaszak, A. Flexible electrode based on mwcnt embedded in a cross-linked acrylamide/alginate blend: Conductivity vs. stretching. *Polymers* **12**, 181 (2020).

Acknowledgements

Author contributions

Y.O., C.P., M.J.F., X.H., J.L., and C.M. designed the research; Y.O. and C.P. fabricated the materials; Y.O., C.P., and M.J.F. performed the experiments; Y.O., C.P., M.J.F., J.L., and C.M. analysed the data; Y.O., C.P., and X.H. produced the demonstration of the soft stingray-inspired swimmer; Y.O., C.P., and J.L. demonstrated the neuromuscular electrical stimulation electrodes; Y.O., C.P., M.J.F., X.H., J.L., and C.M. wrote the manuscript. Y.O., C.P., M.J.F., and C.M. revised the manuscript.

Competing interests

The authors declare no competing interests.